PHYSICAL REVIEW B VOLUME 59, NUMBER 22 1 JUNE 1999-II

Interrelation between orbital polarization and magnetic structure in bilayer manganites

T. Akimoto
Department of Crystalline Materials Science, Nagoya University, Nagoya 464-8603, Japan

Y. Moritomo
CIRSE, Nagoya University, Nagoya 464-8601, Japan
and PRESTO, JST, Chiyoda-ku, Tokyo 102, Japan

K. Ohoyama, S. Okamoto, S. Ishihara, and S. Maekawa
Institute for Materials Research, Tohoku University, Sendai 980-8577, Japan

A. Nakamura
CIRSE, Nagoya University, Nagoya 464-8601, Japan

(Received 10 February 1999)

A-site substitution effects on the magnetic and lattice structure have been investigated for bilayer manganites, $(La_{1-z}Nd_z)_{1.2}(Sr_{1-y}Ca_y)_{1.8}Mn_2O_7$, without changing the e_g-electron concentration ($x=0.4$). The ferromagnetic metallic (FM) phase of the parent $La_{1.2}Sr_{1.8}Mn_2O_7$ ($T_C=120$ K) is suppressed by Nd doping (z), and a paramagnetic insulating (PI) state appears above $z=0.3$. The FM phase is suppressed also by Ca doping (y), but a layered-type antiferromagnetic (A-AF) structure appears above $y=0.3$. We have investigated the stability of the $d_{x^2-y^2}$ (or $d_{3z^2-r^2}$) orbital by Madelung potential calculation based on the structural data, and have found that *orbital polarization* governs the magnetic structure in bilayer manganites.
[S0163-1829(99)50622-X]

Doped manganites with bilayer structure,[1] $La_{2-2x}Sr_{1+2x}Mn_2O_7$, have recently attracted considerable interest due to their ''colossal'' magnetoresistance observed around the insulator-to-metal transition temperature at $x=0.4$. In this layered manganite, the MnO_2 sheets are isolated by two La(Sr)O planes, keeping the two-dimensional networks of the MnO_6 octahedra. Kimura *et al.*[2] have reported tunneling-type magnetoresistance at $x=0.3$, which further attracts current interest of material scientists. On the other hand, Moritomo *et al.*[3] have systematically investigated the magnetotransport properties as well as the magnetic structure of the Nd-doped $(La_{1-z}Nd_z)_{1.4}Sr_{1.6}Mn_2O_7$, and have found the spin-valve magnetoresistance accompanied by antiferromagnetic-to-ferromagnetic transition. Thus, the bilayer manganite shows a variety of magnetotransport properties as well as the magnetic structure,[4] and is a promising material for a magnetoresistive device.

The lattice and magnetic structure for $La_{2-2x}Sr_{1+2x}Mn_2O_7$ have been intensively investigated.[5–8] In this system, the Sr-doping procedure not only (i) decreases the nominal concentration of the e_g electrons, but (ii) significantly releases the static distortion of the MnO_6 octahedra:[9] averaged distortion Δ defined by $\langle d_{\text{Mn-O(out)}}\rangle/d_{\text{Mn-O(in)}}$ decreases from $\Delta=1.03$ at $x=0.3$ to 1.00 $x=0.5$. Such a variation of the static distortion should affect the orbital character of the e_g electrons, and hence the magnetic structure. Moritomo[9] *et al.* have systematically investigated the ground-state properties for $(La_{1-z}Nd_z)_{2-2x}Sr_{1+2x}Mn_2O_7$ ($x=0.4-0.5$), and have found that the ferromagnetic metallic (FM) ground state is replaced by a layered-type antiferromagnetic (A-AF) state beyond $x\approx 0.45$. In this magnetic structure, ferromagnetic MnO_2 sheet alternates along the c axis (intrabilayer coupling is *negative*).[7–9] Such a magnetic structure is interpreted in terms of the $d_{x^2-y^2}$ *orbital polarization*, which causes the FM double-exchange interaction[10] within the MnO_2 sheet and antiferromagnetic superexchange coupling between the adjacent sheets (within the bilayer). A similar A-AF structure has been observed even in the cubic manganites,[11] $R_{1-x}Sr_xMnO_3$ ($R=La_{1-z}Nd_z$), suggesting that the basic physics is similar between the bilayer and cubic manganites. In addition, the aforementioned crossover behavior from FM to A-AF states is qualitatively explained by mean-field calculation of the double-exchange model with explicitly taking account of the degeneracy of the e_g orbital and the anisotropy of the transfer integral.[12] The Sr-doping procedure, however, has two effects, that is, (i) hole-doping and (ii) deformation of the MnO_6 octahedra, which could not be distinguished experimentally.

In this paper, we have investigated *A*-site substitution effects on the magnetic and lattice structure for bilayer manganites, $(La_{1-z}Nd_z)_{1.2}(Sr_{1-y}Ca_y)_{1.8}Mn_2O_7$, without changing the e_g-electron concentration ($x=0.4$). In this system, we can study *purely* lattice effect, excluding the hole-doping effect. We have derived a magnetic phase diagram against Nd and Ca doping: a paramagnetic insulating (PI) state appears above $z=0.3$ (Nd doping), while a layered antiferromagnetic state (A-AF) appears above $y=0.3$ (Ca doping). We further have determined the atomic positions from the neutron powder patterns and investigated the orbital states by calculating the Madelung potentials for the two e_g orbitals. We have found a close interrelation between the magnetic structure and the difference of the Madelung potentials between the two orbitals. This clearly indicates that orbital polarization governs the magnetic structure in bilayer manganites.

TABLE I. Lattice constants and atomic postions at 300 K for $(La_{1-z}Nd_z)_{1.2}(Sr_{1-y}Ca_y)_{1.8}Mn_2O_7$ determined from neutron powder profiles.

y	z	a (Å)	c (Å)	$A2(z)$	O2(z)	O3(z)	Mn(z)	R_{wp}
0.0	0.0	3.86802(9)	20.1052(6)	0.3173(2)	0.1971(2)	0.0955(1)	0.0964(4)	8.57
0.2	0.0	3.8648(2)	20.086(1)	0.3174(3)	0.2002(4)	0.0961(3)	0.0957(7)	12.53
0.3	0.0	3.8623(3)	20.012(1)	0.3175(3)	0.2004(5)	0.0982(4)	0.0920(9)	13.04
0.4	0.0	3.8603(3)	19.941(2)	0.3177(5)	0.2007(6)	0.1021(4)	0.085(1)	14.23
0.0	0.0	3.86802(9)	20.1052(6)	0.3173(2)	0.1971(2)	0.0955(1)	0.0964(4)	8.57
0.0	0.2	3.86325(9)	20.1170(7)	0.3176(2)	0.1980(2)	0.0960(1)	0.0971(4)	8.52
0.0	0.4	3.8558(1)	20.1121(9)	0.3167(2)	0.1984(3)	0.0957(2)	0.0985(5)	11.43

Single crystals of $(La_{1-z}Nd_z)_{1.2}(Sr_{1-y}Ca_y)_{1.8}Mn_2O_7$ were grown by the floating-zone method at a feeding speed of 10–20 mm/h. Stoichiometric mixture of commercial La_2O_3, Nd_2O_3, $SrCO_3$, $CaCO_3$, and Mn_3O_4 powder was ground and calcined twice at 1250−1350 °C for 24 h. The resulting powder was pressed into a rod with a size of 5 mm$\phi\times$60 mm and sintered at 1350 °C for 48 h. The ingredient could be melted congruently in a flow of air. Single crystals, typically 4 mm in diameter and 10 mm in length, were obtained with two well-defined facets, which correspond to the crystallographic ab plane. However, large-y crystals ($y=0.35$ and 0.40) are difficult to grow and we obtained only polycrystalline samples. Rietveld analysis of neutron powder patterns[13] indicate that the investigated compounds were nearly single phase. Neutron-diffraction measurements were performed with the Kinken powder diffractometer for high efficiency and high-resolution measurements (HERMES) installed at the JRR-3M reactor at the Japan Atomic Energy Research Institute, Tokai, Japan.[14] Neutrons with wavelength 1.819 Å were obtained by the (331) reflection of Ge monochromater, and 12′-∞-Sample-18′ collimation. Melt-grown crystal ingots were crushed into fine powder and were sealed in a vanadium capsule with helium gas, and mounted at the cold head of the closed-cycle He-gas refrigerator. The crystal symmetry is tetragonal ($I4/mmm$; $Z=2$) over the whole concentration range. The obtained lattice parameters are listed in Table I, together with the atomic positions. Looking at Table I, one may notice that the A-site substitution effects are different between Nd doping (z) and Ca doping (y); lattice constant a shortens with increasing z, while c shortens with increasing y.

First, let us show temperature dependence of the in-plane component M_{ab} of the magnetization for $(La_{1-z}Nd_z)_{1.2}(Sr_{1-y}Ca_y)_{1.8}Mn_2O_7$. The M_{ab} was measured under a field of $\mu_0H=0.5$ T after cooling down to 5 K in zero field (ZFC), using a superconducting quantum interference device (SQUID) magnetometer. The M_{ab}-T curve for $La_{1.2}Sr_{1.8}Mn_2O_7$ ($z=0.0$) steeply rises below $\approx$120 K, and reaches near the ideal value ($\approx 3.6\mu_B$). The Curie temperature T_C was determined from the inflection point of the M-T curve, and indicated by closed circles in Fig. 1. The magnitudes of M_{ab} at $z=0.2$ and $y=0.2$ approach the ideal value at low temperature, even though T_C shifts to the low-temperature side ($T_C\approx 80$ K). M_{ab} is suppressed with further increasing z (or y), though the M-T curve is reminiscent of ferromagnetism.

To investigate the magnetic structure, we have measured neutron powder patterns. In Fig. 2(a) are shown prototypical examples for $La_{1.2}(Sr_{0.6}Ca_{0.4})_{1.8}Mn_2O_7$; open and closed circles are at 300 K and at 12 K, respectively. Several magnetic reflections appear at 12 K (closed circles). These reflections can all be indexed by either ferromagnetic (indexed by FM) or layered-type antiferromagnetic (indexed by A-AF) structures with spin moment along the in-plane direction.[7,8] The magnetic moments are estimated to be $2.0\pm 0.1\mu_B$ and $1.6\pm 0.1\mu_B$ for the FM and A-AF components, respectively, by Rietveld refinement (thin curve). The magnetization curve [Fig. 2(b)] at 5 K shows a ferromagnetic behavior with saturated moment M_s of $\approx 1.4\mu_B$, which is consistent with the Rietveld refinement. Coexistence of the FM and A-AF components can be ascribed to the spin canting or the electronic phase separation.[15] Some microscopic measurements, however, are necessary to distinguish the two effects. In Table II are listed estimated magnetic moments for the A-AF and FM components of $La_{1.2}(Sr_{0.6}Ca_{0.4})_{1.8}Mn_2O_7$ and $(La_{0.6}Nd_{0.4})_{1.2}Sr_{1.8}Mn_2O_7$. In the Ca-doped compound, the A-AF component appears at 100 K, and then the FM component grows below $\sim$50 K, suggesting a two-step magnetic transition. Consistently, we have observed a two-step transition in the M-T curve measured under a field of $\mu_BH=0.1$ T

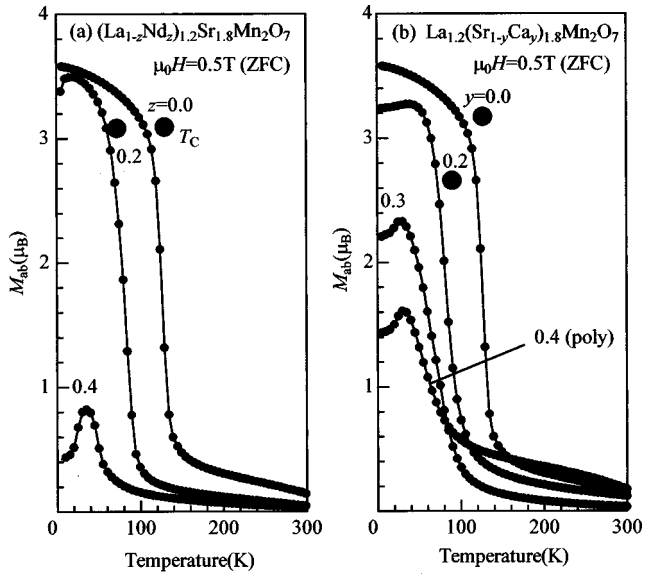

FIG. 1. In-plane component (M_{ab}) of magnetization curves for (a) $(La_{1-z}Nd_z)_{1.2}Sr_{1.8}Mn_2O_7$ (cited from Ref. 16) and (b) $La_{1.2}(Sr_{1-y}Ca_y)_{1.8}Mn_2O_7$. M_{ab} was measured under a field of $\mu_0H=0.5$ T after cooling down to 5 K in zero field (ZFC). The closed circle represents the Curie temperature T_C. Note that an out-of-plane component is mixed in the $y=0.4$ data.

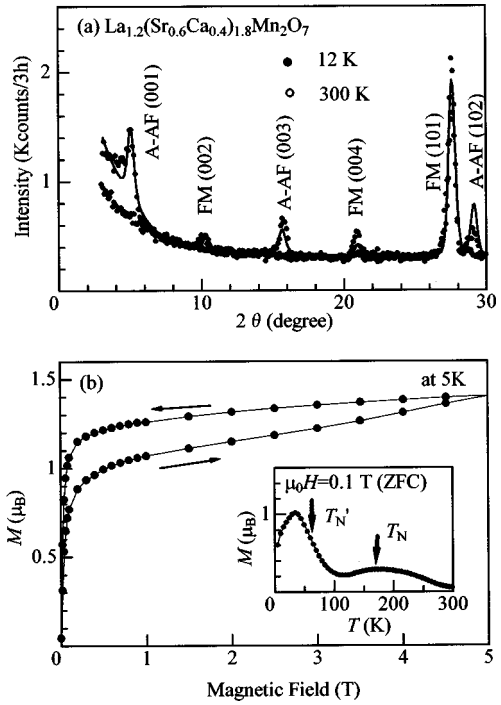

FIG. 2. (a) Neutron powder profiles for $La_{1.2}(Sr_{0.6}Ca_{0.4})_{1.8}Mn_2O_7$ at 300 K (open circles) and at 12 K (closed circles). The curve represents the results of the Rietveld fitting. (b) Magnetization curve for $La_{1.2}(Sr_{0.6}Ca_{0.4})_{1.8}Mn_2O_7$ at 5 K. The inset shows the temperature variation of magnetization M measured under a field of $\mu_0 H = 0.1$ T. T_N and T_N' stand for the Néel and critical temperatures for the mixed phase, respectively.

[inset of Fig. 2(b)]. We have defined the corresponding critical temperatures, i.e., T_N and T_N', as the maximum position and the inflection point of the M-T curve, respectively. By contrast, the Nd doped compound shows a negligible A-AF moment ($\approx 0.5\mu_B$) at 15 K, perhaps due to some extrinsic origin.

The critical temperatures T_C, T_N, and T_N', as determined by the aforementioned techniques, are plotted in Fig. 3. The FM ground state is suppressed with increasing z [see Fig. 3(a)], and eventually the phase disappears. The Ca doping [Fig. 3(b)], however, transforms the FM ground state into the A-AF + FM mixed state. In Fig. 4 are plotted three kinds of the Mn-O bondlengths, i.e., out-of-plane ($d_{\text{Mn-O(1)}}$ and $d_{\text{Mn-O(2)}}$) and in-plane ($d_{\text{Mn-O(3)}}$) bondlengths, determined from neutron powder pattern at 300 K. The data point at $(y,z) = (0.0, 0.0)$ is from Ref. 8. Nd doping [Fig. 4(a)]

TABLE II. Antiferromagnetic (μ_{AF}) and ferromagnetic (μ_F) components for $(La_{1-z}Nd_z)_{1.2}(Sr_{1-y}Ca_y)_{1.8}Mn_2O_7$ determined from neutron powder profiles. Spin directions are within the MnO_2 sheet for both the components.

y	z	Temperature (K)	μ_{AF} (μ_B)	μ_F (μ_B)
0.4	0.0	300	—	—
0.4	0.0	100	0.5±0.1	—
0.4	0.0	50	2.0±0.1	1.6±0.1
0.4	0.0	12	2.0±0.1	1.6±0.1
0.0	0.4	300	—	—
0.0	0.4	15	0.5±0.1	—

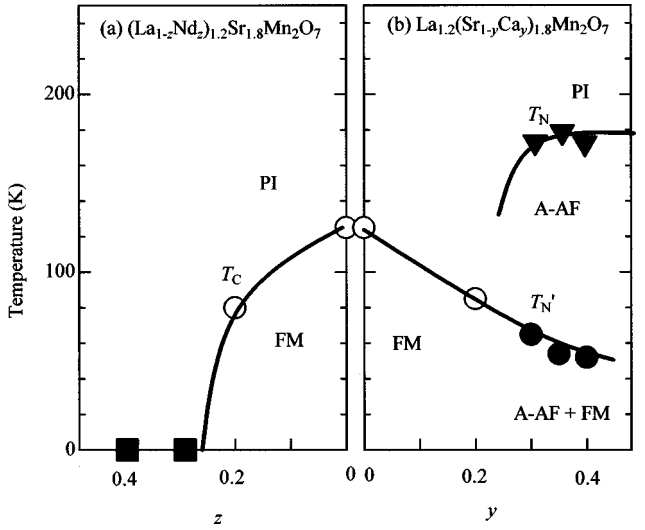

FIG. 3. Magnetic phase diagram for (a) $(La_{1-z}Nd_z)_{1.2}Sr_{1.8}Mn_2O_7$ and (b) $La_{1.2}(Sr_{1-y}Ca_y)_{1.8}Mn_2O_7$. The open circle, closed triangle, and closed circle stand for the Curie temperature T_C, Néel temperature T_N, and critical temperature T_N' for the mixed phase, respectively. FM and A-AF stand for ferromagnetic metallic and layered-type antiferromagnetic states, respectively. The closed square means that no magnetic order is observed down to the lowest temperature.

mainly elongates $d_{\text{Mn-O(1)}}$, and hence stabilizes the $d_{3z^2-r^2}$ orbital. Then, the reduced transfer integral between the neighboring Mn sites within the MnO_2 sheet suppresses the FM phase, as observed.[16] By contrast, complicated behaviors are observed in the case of Ca doping [Fig. 4(b)]; with increasing y, $d_{\text{Mn-O(1)}}$ becomes shorter, but $d_{\text{Mn-O(2)}}$ longer. In other words, the Mn atom in the MnO_6 octahedra moves toward the O(1) site. This is perhaps due to preference of the occupancy of smaller Ca^{2+} ions in the rocksalt layer (within the bilayer), which would deform the MnO_6 octahedron.[17] Such an effect is considered to be unimportant in the Nd-doped compound.

Now, we calculate the Madelung potential for the e_g orbitals and investigate the stability of them in more detail. The

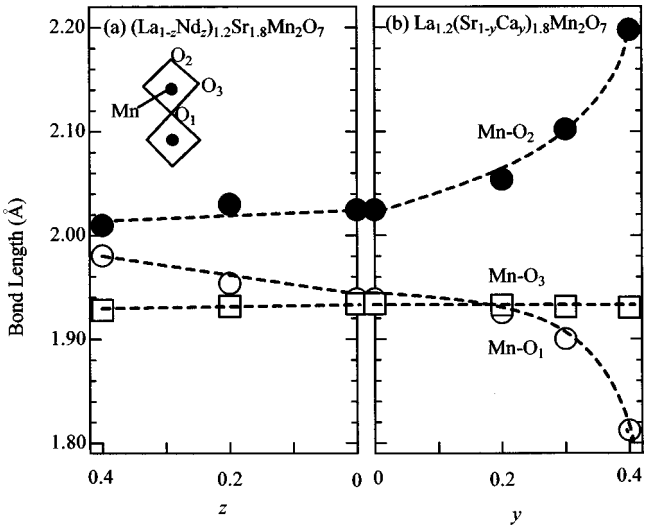

FIG. 4. Mn-O bondlengths for (a) $(La_{1-z}Nd_z)_{1.2}Sr_{1.8}Mn_2O_7$ and (b) $La_{1.2}(Sr_{1-y}Ca_y)_{1.8}Mn_2O_7$. The inset shows two MnO_6 octahedron along the c direction.

Madelung potential acting on a hole in the $d_{3z^2-r^2}$ and $d_{x^2-y^2}$ orbitals are given by[18,19]

$$V(d_{x^2-y^2}) = V(\vec{r}_0 + r_d\hat{x}), \quad (1)$$

and

$$V(d_{3z^2-r^2}) = [V(\vec{r}_0 + r_d\hat{z}) + V(\vec{r}_0 - r_d\hat{z})]/2 \ , \quad (2)$$

respectively. Here $\vec{r}_0$ indicates the position of the Mn ion and $r_d(=0.42$ Å) is the radius where the radial charge density of the Mn $3d$ orbital becomes maximum. $\hat{x}$ and $\hat{z}$ are the unit vector along the in-plane and interplane Mn-O bonds, respectively. Valences of the charge at *A*, *B*, and oxygen sites are assumed to be $+2.4$, $+3.4$, and -2, respectively, and the conventional Ewald method is used. Based on the structural data obtained by the neutron-diffraction experiment, we calculate the difference of the Madelung potential between two e_g orbitals: $\Delta V = V(d_{3z^2-r^2}) - V(d_{x^2-y^2})$.

Finally, we plotted the critical temperatures, i.e., T_C, T_N, and T_N', against ΔV (see Fig. 5). Critical temperatures from both the Nd-doped and Ca-doped compounds can be plotted on the same phase diagram, as a function of the stability of the orbital. If one sees the phase diagram from right to left (the $d_{x^2-y^2}$ orbital polarization increases), the magnetic structure changes from PI to FM, and finally the A-AF state appears. The A-AF magnetic structure originates from the increased $d_{x^2-y^2}$ *orbital polarization*, which causes the FM double-exchange interaction within the MnO_2 sheet and antiferromagnetic superexchange coupling between the adjacent sheets. Thus, we have confirmed without ambiguity that the orbital polarization governs the magnetic structures in bilayer manganites.

The authors are grateful to K. Nemoto for his help in the measurement of neutron powder diffraction. We also thank M. Kubota, K. Hirota, and H. Yoshizawa for informing us of unpublished structural data for $La_{1.2}Sr_{1.8}Mn_2O_7$. S.O. and T.A. acknowledge the financial support of JSPS. This work was supported by a Grant-In-Aid for Scientific Research from the Ministry of Education, Science, Sports and Culture, from Precursory Research for Embryonic Science and Technology (PRESTO), Japan Science and Technology Corporation (JST).

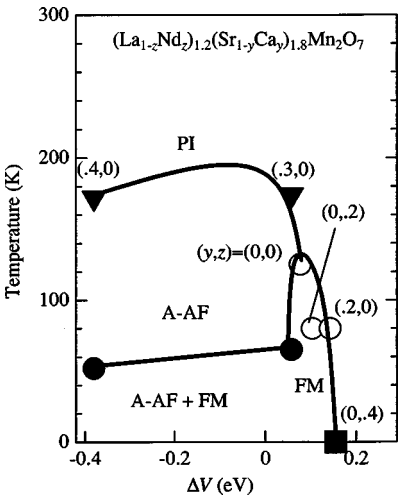

FIG. 5. Magnetic transition temperatures against the difference of the Madelung energies $\Delta V[=V(d_{3z^2-r^2})-V(d_{x^2-y^2})]$, where $V(d_{3z^2-r^2})$ $[V(d_{x^2-y^2})]$ is the Madelung energy for the $d_{3z^2-r^2}$ $(d_{x^2-y^2})$ hole. The $d_{3z^2-r^2}$ orbital polarization increases as ΔV increases. The open circle, closed triangle, and closed circle stand for the Curie temperature T_C, Néel temperature T_N, and critical temperature T_N' for the mixed phase, respectively. FM and A-AF stand for ferromagnetic metallic and layered-type antiferromagnetic states, respectively.

[1] Y. Moritomo, A. Asamitsu, H. Kuwahara, and Y. Tokura, Nature (London) **380**, 141 (1996).
[2] T. Kimura, Y. Tomioka, H. Kuwahara, A. Asamitsu, M. Tamura, and Y. Tokura, Science **274**, 1698 (1996).
[3] Y. Moritomo, K. Ohoyama, and M. Ohashi, Phys. Rev. B **59**, 157 (1999); Y. Moritomo and M. Itoh, *ibid.* **59**, 8789 (1999).
[4] Y. Moritomo, Aust. J. Phys. (to be published).
[5] J. F. Mitchell, D. N. Argyriou, J. D. Jorgensen, D. G. Hinks, C. D. Potter, and S. D. Bader, Phys. Rev. B **55**, 63 (1997).
[6] D. N. Argyriou, J. F. Mitchell, C. D. Potter, S. D. Bader, R. Kleb, and J. D. Jorgensen, Phys. Rev. B **55**, R11 965 (1997); D. N. Argyriou, J. F. Mitchell, J. B. Goodenough, O. Chmaissem, S. Short, and J. D. Jorgensen, Phys. Rev. Lett. **78**, 1568 (1997).
[7] K. Hirota, Y. Moritomo, H. Fujioka, M. Kubota, H. Yoshizawa, and Y. Endo, J. Phys. Soc. Jpn. **67**, 3380 (1998); Y. Moritomo, A. Nakamura, K. Ohoyama, M. Ohashi, and K. Hirota, *ibid.* **68**, 631 (1999).
[8] M. Kubota, H. Yoshizawa, K. Hirota, H. Fujioka, Y. Endo, and Y. Moritomo, J. Phys. Chem. Solids (to be published); M. Kubota, H. Fujioka, K. Hirota, K. Ohoyama, Y. Moritomo, H. Yoshizawa, and Y. Endo (unpublished).
[9] Y. Moritomo, Y. Maruyama, T. Akimoto, and A. Nakmura, J. Phys. Soc. Jpn. **67**, 405 (1998), and references cited therein.
[10] P. W. Anderson and H. Hasagawa, Phys. Rev. **100**, 675 (1955).
[11] T. Akimoto, Y. Maruyama, Y. Moritomo, A. Nakamura, K. Ohoyama, M. Ohashi, and K. Hirota, Phys. Rev. B **57**, R5594 (1998); Y. Moritomo, T. Akimoto, A. Nakamura, K. Ohoyama, and M. Ohashi, *ibid.* **58**, 5544 (1998).
[12] R. Maezono, S. Ishihara, and N. Nagaosa, Phys. Rev. B **57**, R13 993 (1998); **58**, 11 583 (1998).
[13] F. Izumi, in *The Rietveld Method*, edited by R. A. Young (Oxford University Press, Oxford, 1993), Chap. 13; Y.-I. Kim and F. Izumi, J. Ceram. Soc. Jpn. **102**, 401 (1994).
[14] K. Ohoyama, T. Kanouchi, K. Nemoto, M. Ohashi, T. Kajitani, and Y. Yamaguchi, Jpn. J. Appl. Phys., Part 1 **37**, 3319 (1998).
[15] For example, see S. Mori, C.-H. Chen, and S.-W. Cheong, Phys. Rev. Lett. **81**, 3972 (1998).
[16] Y. Moritomo, Y. Maruyama, T. Akimoto, and A. Nakamura, Phys. Rev. B **56**, R7057 (1997).
[17] R. Seshadri, C. Martin, A. Maigna, A. Hervieu, M. Raveau, and C. N. R. Rao, J. Mater. Chem. **6**, 1585 (1996).
[18] Y. Ohta, T. Tohyama, and S. Maekawa, Phys. Rev. B **43**, 2968 (1991).
[19] S. Ishihara, S. Okamoto, and S. Maekawa, J. Phys. Soc. Jpn. **66**, 2965 (1997).